Conceptual design and evaluation of blended-wing-body aircraft

Brown, Malcom; Vos, Roelof

DOI
10.2514/6.2018-0522

Publication date
2018

Document Version
Accepted author manuscript

Published in
AIAA Aerospace Sciences Meeting

Conceptual Design and Evaluation of Blended-Wing-Body Aircraft

Malcom Brown* and Roelof Vos†

Delft University of Technology, 2629HS Delft, the Netherlands

Blended wing body (BWB) aircraft represent a paradigm shift in jet transport aircraft design that promise benefits over conventional aircraft. A method is presented to enable the conceptual design of BWB aircraft, enabling comparison studies with tube-and-wing aircraft (TAW) based on the same top-level requirements and analysis fidelity. The aim of this work is to make comparative studies between the blended-wing-body aircraft and its conventional tube-and-wing counterpart based upon the same design requirements at conceptual level. By developing a novel geometric parametrisation of the blended wing body, the design possibilities have been increased while maintaining straightforward shaping manipulation and robustness. The mass estimation methods that have been implemented are verified and validated to be within approximately 5% of reference blended wing bodies. Drag estimations perform less accurately with drag being overpredicted by approximately 20%. The cause of this over prediction was largely due to empirical corrections for miscellaneous and unaccounted drag sources as well as induced drag predicted by a vortex-lattice method. Test-case BWB and TAW aircraft were formed in the 150, 250 and 400 passenger classes. The comparisons of the resulting aircraft show that the blended wing body have reduced mass, improved aerodynamic efficiency and higher fuel economy. Trends also show that the improvements over tube-and-wing aircraft increase with aircraft size.

I. Introduction

Blended wing body (BWB) aircraft are one of the unconventional aircraft that are currently being intensely investigated by academia and the aerospace industry. They are a promising aircraft concept that have many important advantages over the conventional tube and wing (TAW) aircraft such as higher aerodynamic efficiency leading to lower fuel burn and emissions, lower noise emission and overall lower operational cost to airlines and operators.[1] These factors are becoming increasingly important in modern society and trends in aircraft design and operation have reflected this.

Design studies of the BWB have tended to focus on specific aircraft which are often based on a baseline geometry, due, in part, to the difficulty of sizing a feasible and consistent BWB in the absence of empirical design methods. Rapid evaluation of changes to top level requirements (TLR) or geometric layout at conceptual level is challenging and often not possible with current design philosophies. The nature of conceptual aircraft design calls for rapidly executable methods with acceptable accuracy, on which requirement satisfaction, layout, dimensioning, performance and mass budgets can be based. With improved synergy between established design methods and computer-based methods, this task is becoming easier and yields good results.[2] Computer-based design methods have been used extensively in the past. However, openly available programs tend to be limited in their ability to model unconventional designs, especially the BWB.[3] Furthermore, there is still a lack knowledge as to the comparison of BWB aircraft to their TAW counterparts, designed to the same objectives, specifications and fidelity. The ability to design, analyze and compare both conventional TAW and BWB aircraft of various missions and configurations, using similar methods, would allow for an increased understanding of the feasibility of the BWB concept, as a whole, over a wide design space.

*Researcher, Faculty of Aerospace Engineering, Kluyverweg 1, Delft

†Assistant Professor, Aerospace Engineering, r.vos@tudelft.nl, Senior member AIAA.

In 2012, the Flight Performance and Propulsion department at TU Delft identified these needs and responded by creating the Aircraft Design Initiator (in short *Initiator*).[4] This conceptual aircraft design program is able to design and analyze passenger jet airliners based on top level requirements and limited input parameters. It makes use of semi-empirical and semi-analytical design methods in an iterative convergence loop to select an overall consistent and feasible design. Conventional as well as unconventional aircraft are implemented although it lacked proper functionality for blended-wing-body aircraft. This presents an opportunity for improvement of the Initiator by implementing the BWB into its design and analysis routines.

The goal of this study is to develop and implement design methods that allow for the side-by-side comparison of BWB and TAW aircraft and apply these methods to three different classes of aircraft to quantify the key performance indicators such as maximum take-off mass, aerodynamic efficiency, and fuel consumption over the harmonic mission. In the subsequent sections, geometry modeling (Sec II), analysis methods (Sec. III), verification and validation (Sec. IV), and the three case studies (Sec. V) are presented. The paper closes with conclusions (Sec. VI) on the expected benefits of the designed BWB aircraft over their TAW counterparts.

II. Geometry Modeling

The process followed in the build up of the geometry model of the BWB is shown in Figure 1. Each of the rectangular blocks represents a process in Matlab, while each trapezoidal block represents data. In order to simplify methods and implementation, the BWB geometry is first defined in the 2D XY-plane (planform shape). The Z components of the geometry are then determined from separate routines and concatenated to the XY data, forming the complete three-dimensional geometry. This decouples the shaping methods and allows for alterations to be made to each shaping routine individually. This process is further elaborated in the subsections below.

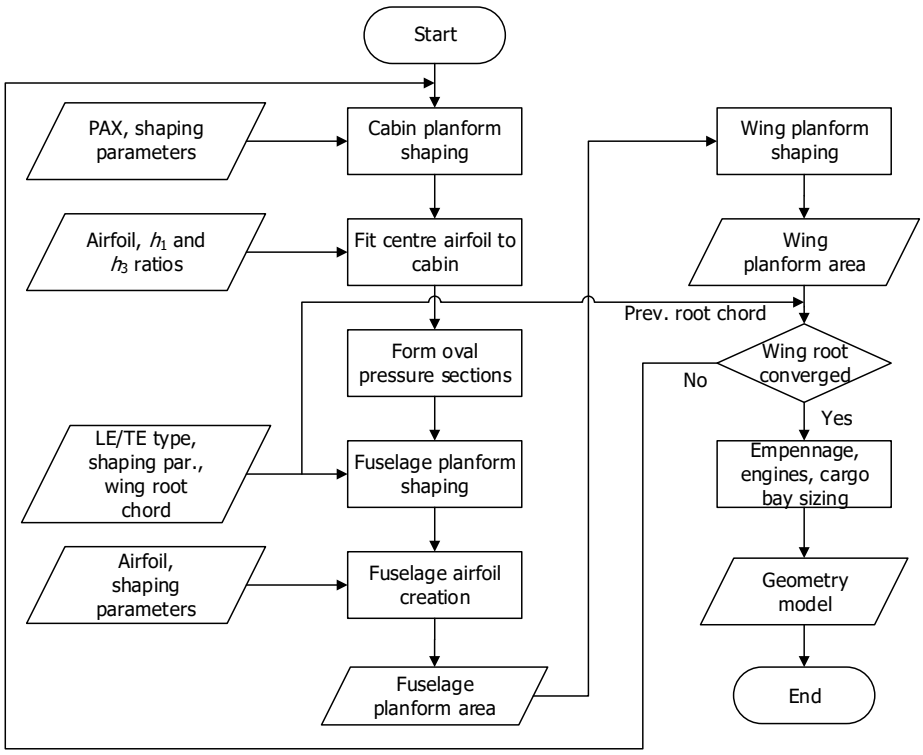

Figure 1 Process followed during geometry estimation of the BWB in the Initiator

A. Cabin Geometry

The build up of the geometry begins with the cabin. The cabin planform consists of tapered section in the front, section of constant width in the middle and an additional aft tapered section, which is added to the conventional *home-plate*[5] BWB cabin shape giving increased shaping possibilities and a tighter fit of the cabin. The parametrization is shown in Figure 2. The length of the center and aft section are linked to the length of the first section l_0 through the length ratios u_1 and u_2 respectively. The widths of these sections are also linked to l_0 by the width-to-length ratios v_1 and v_2 respectively. This parametrization allows for the variation of the shape of each section independent of the other sections and overall cabin size, giving rise to easier and more intuitive manipulation of the cabin shape and unitary scaling between different sized BWB cabins. The length and width ratios and the cockpit width w_{cp} are the five input variables that fully determine the cabin planform shape. The size of the cabin is determined from the required number of passengers (pax) and an empirical passenger-per-area ratio giving the required floor area S_{floor}. Length l_0 is determined by solving the following equation from which the lengths and widths of the sections are evaluated with their length and width ratios:

$$S_{\text{floor}} = \left[0.5v_1 + u_1v_1 + 0.5u_2\left(v_1 + v_2\right)\right] {l_0}^2 + 0.5w_{\text{cp}}l_0 \tag{1}$$

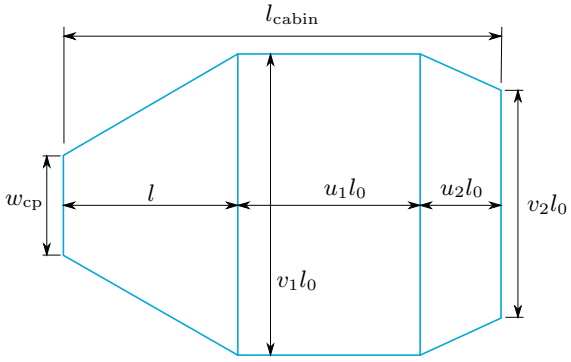

Figure 2 Parametrisation of the cabin floor, note l_{cabin} is not a variable but a result of the parametrisation.

Seating layout is applied to the sized cabin planform, an example of which is shown in Figure 3. This is done by placing predefined seats in rows as wide as the cabin locally allows while complying with §CS 25.817 (3 seats abreast). Emergency exits are determined based on the number of pax and placed with the maximum spacing in accordance with §CS25.807, thereby allocating the number of exits on the sides of the fuselage as shown. Feasibility of the exits at the same fuselage station (FS) as the wing can be brought into question as it is expected to be difficult to place exits here from a structural point of view. However, this has not been taken into account in this study. Galleys and lavatories are placed at these exits (if required) and stretched across the span of the cabin due to the use of conventional TAW aircraft methods. Diagonal aisles, as commonly seen in BWB cabin designs,[6] are not implemented. However, these are not always necessary[7] and depend on the emergency exit location.

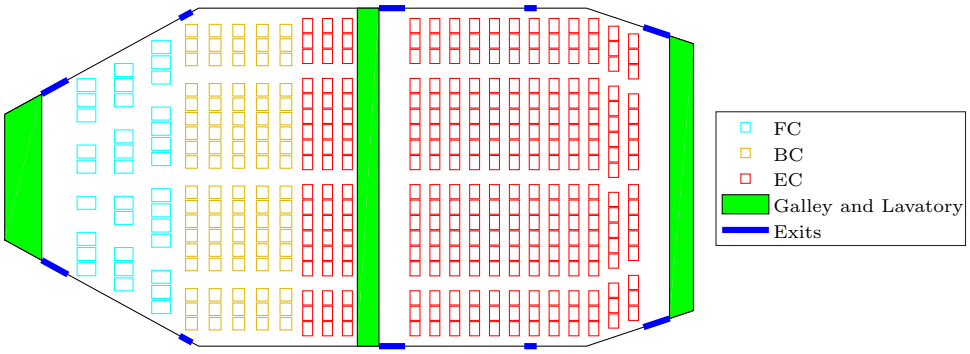

Figure 3 Seat placement and cabin layout of a typical BWB in the Initiator

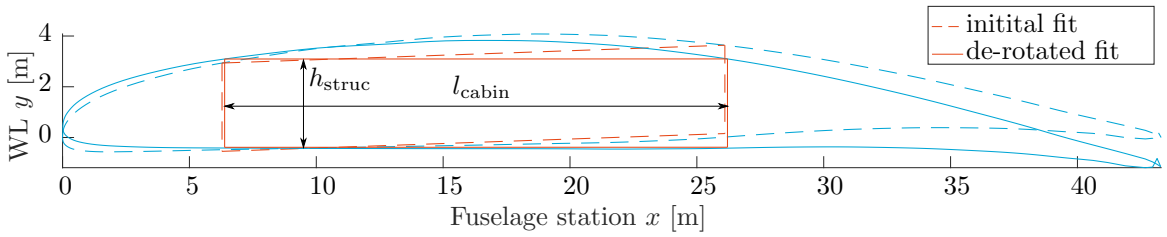

Figure 4 Fitting of the cabin outline within the centre airfoil showing de-rotation of the cabin

All BWB aircraft use an airfoil shape of some kind over the center body. The fuselage definition used in the Initiator requires the airfoil shape at the center section as input. Therefore the previously sized cabin is fitted within this input center airfoil. This is done by scaling the chord of the airfoil and optimizing the fit of the cabin box defined by the required overall cabin length l_{cabin} and cabin structural height h_{struc}. The waterline datum definition within the Initiator is the cabin floor and as such needs to be placed at $Z = 0$ and set level. The airfoil is then moved up and down for best fit. Rotating the airfoil can also lead to a better fit, sometimes reducing wetted area considerably. This does however set the incidence angle of the fuselage airfoil with respect to the cabin. The cabin deck angle needs to be a reasonable value in cruise ($\leq 3°$) and needs to be checked once the cruise angle of attack (AoA) is known. The results of this process are shown in Figure 4.

The cabin pressurization structure is formed using the oval fuselage definition[8,9] and is shown with the main design parameters in Figure 5. The three discrete but tangent arcs result from the local heights h_1 and h_3 and the local cabin floor width w_{cabin}. The structural height is the total height of the section and is used to fit the airfoil at the most fore and aft section as, shown in Figure 4. Importantly, h_1 and h_3 cannot be zero, as this would cause the radius of the top or bottom arcs to be infinite, leading to a flat panel which is inefficient at carrying the out-of-plane bending loads due to pressurisation. As the radius of the arc tends towards infinity, the required thickness of the structural panel increases, and so too does the weight.[10] The oval section is determined at each of the four discrete cabin corner points, forming the total pressure shell as shown in Figure 6.

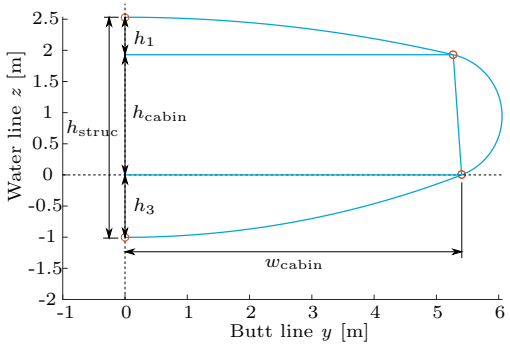

Figure 5 Definition of the oval fuselage half cross section on the YZ-plane

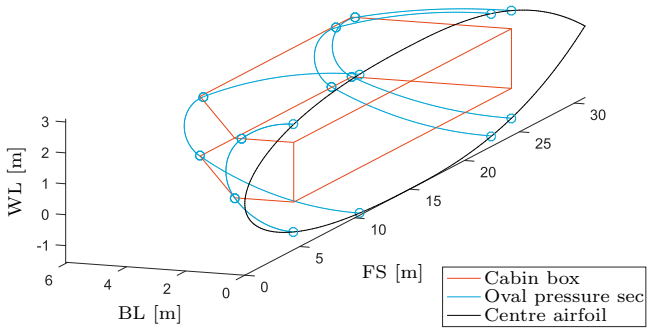

Figure 6 Half oval fuselage sections fitted to the centre airfoil and cabin corner points giving the 3D pressure shell geometry

B. Fuselage Planform Shaping

Nose and tail sections are added to the cabin which then form the complete fuselage. The planform shaping of the fuselage is performed in two steps: the first is to choose the overall shape of the leading edge (LE) and TE and the second is to refine the planform shape with specific shaping parameters. Three global options for planform shape have been implemented and are shown in Figures 7a, 7b and 7c. Different types of LE and TE can be mixed, for example a *structural* LE with a *straight* TE, which allows for more design freedom. These options allow a vast array of different BWB planform shapes to be created and analysed using the

same methods, which is typically not possible with other design tools.

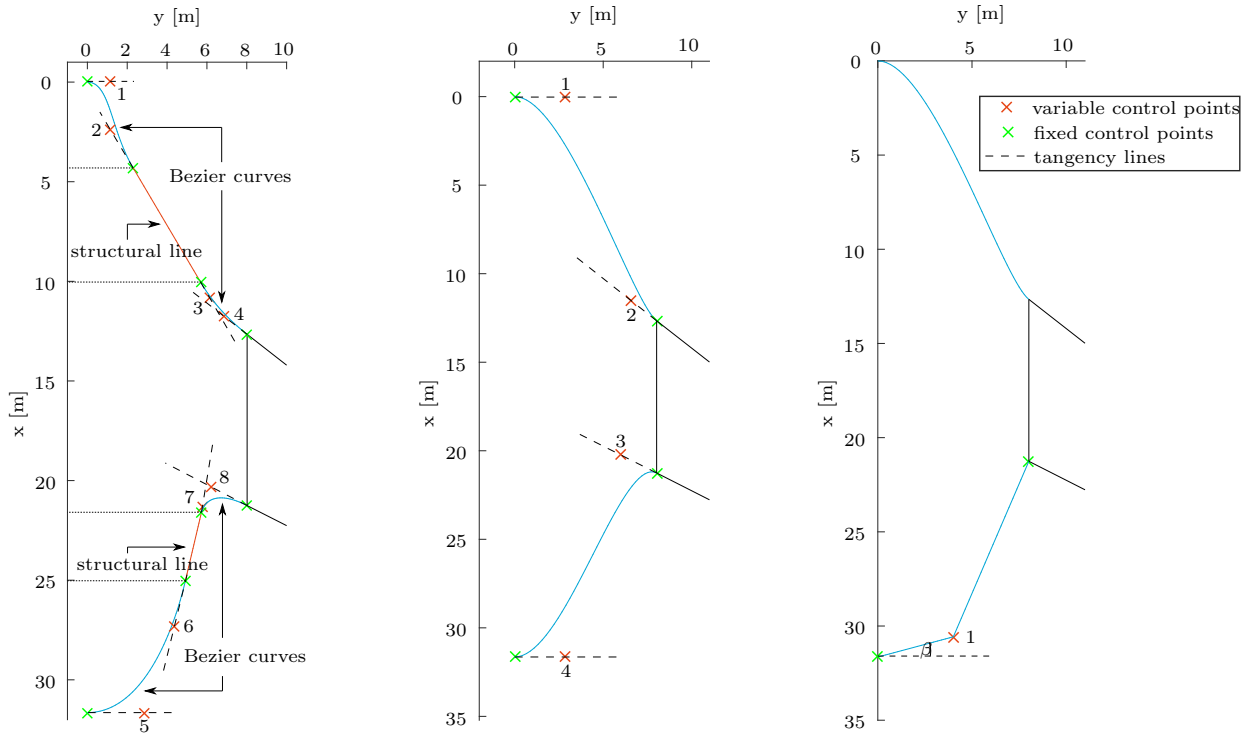

(a) *Structural* LE and *structural* TE type

(b) *Loose* LE and *loose* TE type

(c) *Straight* TE type

Figure 7 Parametrisation of the three planform parametrizations

The rationale behind the *structural* LE or TE type (Figure 7a) is that the structure of the pressure shell forms part of the LE or TE without the need for an aerodynamic fairing. This should reduce the part count, structural mass and manufacturing costs. It also has a lower planform and wetted area, leading to a more compact design and reduced friction drag. It can however have an overall aerodynamic penalty because the airfoil shape is fully dependent on the pressure shell shape. The nose section is formed from a Bezier curve which begins blunt at the fuselage nose (centre airfoil LE) and ends tangent to the proceeding straight structural line. This line is defined by the outer widths of the pressure shell at the first and second oval sections. Joining this line to the outer wing apex is another Bezier curve, which begins tangent to the pressure shell and ends tangent to the outer wing LE. The TE line is constructed in a similar fashion. Variables are scaled such that input values between zero and one can be used, independent of the size of the BWB, which increases the ease of use.

The second option is the *loose* LE or TE, shown in Figure 7b, where the path of the LE or TE is independent of the pressure shell. This option requires some form of fairing to link the LE or TE to the pressure shell, forming a double skin. This increases the part count, structural mass and wetted area. More curved panels are used, potentially leading to a negative impact on manufacturability. The main advantage is that an aerodynamically shaped cap is added to the nose and tail of the fuselage airfoils, forming a more conventional airfoil shape. These shapes can subsequently be altered to improve the aerodynamics of the fuselage, as will be further described in Section C. Parametrization of the *loose* type is done in a straightforward manner and is based on the work of Kanazaki et al.[11] A single Bezier curve is constructed from the nose of the fuselage to the outer wing apex. It begins blunt at the nose (centre airfoil LE) and ends tangent to the outer wing LE. It is controlled by 4 control points as shown in Figure 7b. Finally, a *straight* TE can be used, shown in Figure 7c. This is similar to the *loose* option, except for the fact that

straight lines are used. The TE is formed from two straight lines which end sharply at the centre airfoil TE and outer wing TE. The location of the kink is set by the Y coordinate of the variable control point and the angle of the TE.

The last topic concerning the sizing of the planform is the link to the fuselage airfoil shapes which are placed at a spanwise location in longitudinal direction. More explanation of the actual airfoil fitting is provided in the next section but the link with planform shaping comes in the Z location of the LE and TE. The planform shape (LE and TE curves) has only been defined on the XY-plane. Due to actual airfoil shape and twist, the LE and TE do not necessarily fall on this plane, i.e. $Z = 0$. Since the airfoil shape is governing, the previously defined LE and TE curves need to coincide with the airfoil LE and TE in the Z-coordinate. This is done by creating straight lines, in the YZ-plane, joining each actual airfoil LE and TE, respectively, and concatenating these Z-coordinates to the XY-coordinates previously found, thus creating the final LE and TE line in three-dimensional space.

It can be seen in Figures 7a - 7c that the geometry of the outer wing is required as input for the planform shaping of the fuselage. This forms the coupling between the sizing of the fuselage and of the outer wing, shown in Figure 1, and is one of the main couplings that distinguishes the BWB design from the TAW design. The underlying theoretical reason for this coupling is the inclusion of the fuselage planform area in the total lifting surface area required to achieve the design wing loading.[1,12,13] Since the wing geometry is not yet known on the first iteration, an initial guess for the basic wing design parameters is made. This is done for an outer wing of 40 % of the reference wing area as this was found to be a good starting point which minimized the computation time needed to reach convergence. The actual outer wing geometry is used, instead of these guess values, once it is known from subsequent iterations. Thus, once the method converges, both the fuselage and outer wing geometry agree. The most important wing parameter, which influences the fuselage shape, is the outer wing root chord because it determines the end point of the TE. It is for this reason that the wing root chord is chosen as the convergence parameter for the loop in Figure 1. Iterations continue until the difference between the root chords is less than 1mm. The planform area of the fuselage, as defined by the area between the LE and TE curve on the XY-plane, is required and is calculated with suitably discretised spanwise trapezoids. This planform area is used as the fuselage reference area and is also used as the contribution of the fuselage to the required wing area from the chosen wing loading.

C. Fuselage Airfoil Generation

As stated before, the oval fuselage concept is single skinned, hence the longitudinal airfoil shape is largely determined by the shape of the fuselage. This can be more clearly seen in Figure 8. A cap is added to the nose or tail of the airfoil if a *loose* or *straight* LE or TE is chosen. If not, the pressure shell forms the whole airfoil. Therefore the pressure shell is sectioned in the XZ-plane (free stream direction) at suitable spanwise positions. The number and spanwise position of these sections are chosen by the designer. Increasing the number of sections does not necessarily improve performance or accuracy as these airfoil sections are also the ones used in the aerodynamic analyses described in Section C. It was found that too sparse or too dense an airfoil distribution can negatively impact paneling and accuracy in the aerodynamic solver. Four linearly distributed (spanwise) airfoil sections were found to give smooth transitions in geometry with acceptable accuracy and computational time.

If required, the caps shown in Figure 8 are formed from Bezier curves based upon the successful method developed by Hileman et al.[14] Upper and lower surfaces are designed separately, each with their own Bezier curve controlled by four control points. The cap is made to end tangent to the pressure shell with the intersection point being determined from the first point at which the resulting Bezier curve is convex. Convexity is chosen as the determining factor as this proved to be the most robust method tested in terms of finding the intersection between pressure shell and airfoil cap. Resulting airfoil shapes are smooth and consistent. However, convexity does limit the airfoil shapes that can be formed. Concave airfoils are not possible. The middle two control points of each Bezier curve are variable based on shaping parameters. They represent the nose bluntness and curvature of the cap at the LE and the boat tail angle and curvature at the TE. This gives a simple and efficient way of manipulating the cap shape with only eight parameters for a full airfoil. These caps are then concatenated to the pressure shell sections at the intersection points and form the final airfoil. This divides the fuselage into aerodynamic sections and creates the airfoil stack which is used for the aerodynamic analysis of the fuselage.

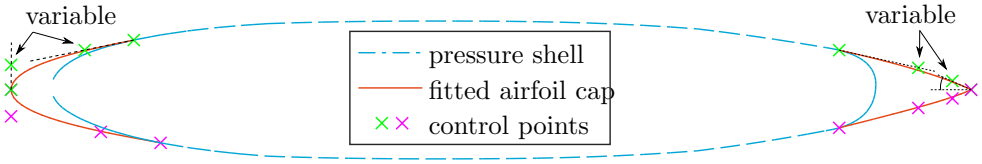

Figure 8 Formation of the fuselage airfoil from the combination of the sectioned pressure shell and a fore and aft cap

D. Outer Wing Sizing

The outer wing is sized based on the completed fuselage geometry, as shown in Figure 1. The outer wing is a straight trapezoidal wing. Reference area for the BWB is defined as the total gross planform area of the fuselage and outer wings:[12,15]

$$S_{\text{ref}} = S_{\text{f}} + 2S_{\text{w}}, \tag{2}$$

where S_{f} is the previously-defined fuselage reference area and S_{w} is the planform area (in the XY-plane) of one of the trapezoidal outer wings. The reference wing area, S_{ref}, is determined from the design wing loading discussed Section B. The gross aspect ratio is used as the aspect ratio A unless otherwise stated:

$$A = \frac{b^2}{S_{\text{ref}}}, \tag{3}$$

where b is the total reference wing span from wing tip to wing tip. Aspect ratio is defined a priori by the designer and kept constant throughout the design process. The longitudinal and lateral positioning of the wing root apex is also set by input fractions of the fuselage length and width, respectively. Sweep angle of the LE is initially determined from wave drag limitations using simple sweep theory and refined by the Korn equation.[16,17] The minimum required sweep angle is later on in the design process also computed during the stability analysis where the larger of the two is limiting. Wing taper ratio λ_{w} is determined from a statistical relation between sweep angle and taper ratio for straight trapezoidal wings in Torenbeek.[18] Predefined airfoils are placed at the root and tip sections. Airfoils chosen for the outer wing are the same as for conventional TAW aircraft and are supercritical sections based on the Boeing 737 kink and outboard airfoils[19] following the results of Sargeant et al.[20]

E. Aircraft Layout

After convergence of the fuselage and wing is achieved the rest of the aircraft geometry is estimated. This includes the vertical stabilizers, engines, landing gear and cargo bay. Vertical stabilizer areas are sized using the volume coefficient method.[21] Volume coefficients are slightly lower than for conventional aircraft following the results of Larkin.[22] Winglets can also be used but it is up to the designer to chose adequate input parameters for their sizing. The sweep angle is set 5% larger than the outer wing sweep to prevent flow separation at design dive Mach numbers as for conventional aircraft.[19,22] Conventional turbofan engines have been chosen for the current BWB investigations as the objective is to compare the BWB to conventional TAW aircraft. Engines are sized based on the engine length and diameter that results from statistical fits through reference engine data for the required thrust per engine.[23] It is chosen to locate the engines in pods over the rear of the fuselage to help balance the aircraft, shield noise and limits foreign object damage.[1,24] It also lends itself well to structural integration as the strengthened rear bulkhead is located roughly underneath the pylons and gives the opportunity for structural synergy. Engines are placed at the XYZ-coordinates determined from input fractions of the fuselage length, diameter and height respectively. Installation drag penalties due to interference are taken into account based on the results of reference[25] which found that a drag penalty of 1.4% is achievable. A 2% unaccounted drag penalty is already added to the zero-lift drag of the aircraft, as discussed in Section C, and it is assumed that this includes the increase in drag due to installation of the engine.

Landing gear layout and design is done following the procedures given by Roskam[26] as for TAW aircraft. This is suitable for the BWB as the landing gear needs to perform to the same ground handling and airport specifications as TAW aircraft. The landing gear is placed and sized by the following constraints from:[26] aft tip-over, lateral tip-over, rotation tail strike, nacelle ground clearance, wheel-to-fuselage clearance and the

minimum and maximum nose gear load. Both the nose and main gear are placed on the fuselage as it is commonly wide and long enough to accommodate the gear at suitable locations.[12,27,28] It is proposed that the main gear retracts underneath the cabin in the thick underbelly. There is sufficient thickness around the center of the fuselage for the width of the main gear but a manual check for this condition must be made. The cargo bay is also located underneath the passenger cabin in the pressurized oval shell. The oval fuselage lends itself well to the placement of cargo in the BWB concept. The large uninterrupted space allows for efficient placement of cargo containers. Firstly, the available cargo floor area is determined, based on each ULD's height with suitable margins, by intersecting the pressure shell at the appropriate waterline. ULDs of the current type and dimension are placed in rows according to the local width of the intersected floor. Total available cargo mass is checked versus the required cargo mass, indicating if the current ULD is feasible. If no ULDs are feasible bulk cargo is placed. If the use of bulk cargo is not permissible, the user is required to modify the fuselage shaping such that thickness is increased and sufficient ULDs can be placed. This can be achieved by increasing the h_3 parameter of the cabin (Figure 5), by using a thicker center airfoil or by modifying the cabin planform shape such that a longer cabin is sized. A longer cabin will increase the center airfoil chord length, making the airfoil thicker and so too increasing the height underneath the cabin.

III. Design and Analysis Procedures

The implemented mass, drag and longitudinal stability and control analyses methods are detailed in this section. Simulation of the missions for which the aircraft is designed is also beneficial in order to establish a more accurate estimation of the fuel required to fly each mission. This procedure is already implemented and verified by Wortmann *et al.*[29] and is suitable for the BWB as it is not configuration specific. These design and analysis procedures allow for a comprehensive analysis of the key performance indicators of the BWB in order to form preliminary conclusions as to its comparison to TAW aircraft. Implemented methods are of similar fidelity to those for TAW aircraft in staying with the goal of the work.

A. Mass Estimation

Mass estimations within the Initiator are done in steps of increasing fidelity in the form of the common Class I and Class II philosophy. Class I entails estimation of the operational empty mass (OEM) and the required fuel mass which, together with the payload mass (PM) from TLRs, gives the maximum take-off mass (MTOM). OEM is estimated using a linear least-squares fit through reference BWB data for payload mass vs. OEM. Fuel fractions (FF), and subsequently fuel mass (FM), are calculated using the lost range parameter formulation of Torenbeek.[30,31] Reserve fuel is also determined from the specified diversion range and loiter time. The MTOM is then determined from the following equation:

$$\mathrm{MTOM} = \frac{\mathrm{PM} + \mathrm{OEM}}{(1 - \mathrm{FF}_{\mathrm{tot}})} \tag{4}$$

This Class I MTOM is used in combination with the wing loading and thrust-to-weight ratio from Section B to create the geometry mentioned in Section II.

Once the geometry is known, the Class II mass estimation is performed. This determines the aircraft component masses based on the aircraft's dimensions, geometry parameters, TLRs and airworthiness requirements. There are a limited number of methods available in open literature which are applicable to BWB, owing to their unique and complicated structures. Airframe structural mass estimation is performed first. As successfully used by Okonkwo,[2] the method of Howe[10] has been chosen for implementation due to its ability to model and take geometrical differences into account, its relative accuracy for being a semi-analytical method, and its very short execution time. Furthermore, the method has appropriate corrections for the use of composite materials which are expected to form an important design choice for the BWB,[10],[32].[33] Using this method, the mass of the outer wing, fuselage and winglets (if used) are determined. In order to do this, the structural idealization of the geometry used in Howe[10] has been applied to the BWB geometry formed by the Initiator. The Initiator version of this idealization is depicted in Figure 9 and shows that it is in agreement with that of Howe. Howe's structural mass calculations do not include estimations of the vertical tail mass if one is used. Since the vertical tail is similar to conventional aircraft, the same method as for TAW from Torenbeek[18] is used.

The mass of the remaining aircraft components, such as landing gear and fixed equipment, are determined

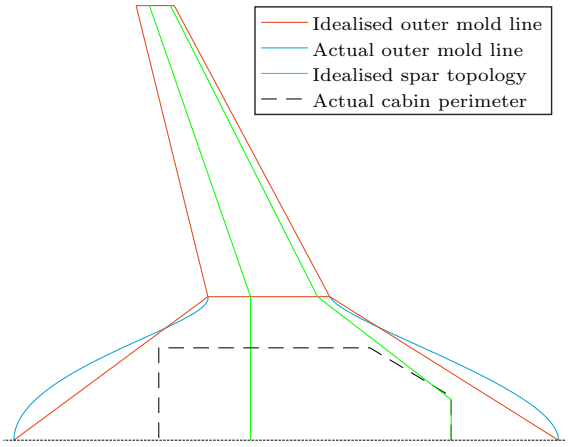

Figure 9 Implementation of the idealisation of[10] to the BWB in the Initiator

from Torenbeek's Class II method[18] and are also used for TAW aircraft. This method has been shown to be more accurate than other methods of similar fidelity.[34]

B. Requirement Analysis and Design Space

A design point needs to be chosen for the aircraft in terms of wing loading and thrust loading. This is done by analysing the input TLRs and airworthiness requirements as is done for conventional aircraft. The method makes use of the relations found in Roskam[26] and the implementation has been discussed by Slingerland.[35] The requirements which are met are as follows: take-off and landing distance, minimum climb gradient according to §FAR25.111c, §FAR25.119 and §FAR25.121a-d, thrust required in cruise, buffet in cruise at a load factor of 1.3, maximum wingspan based on airport requirements and fuel volume requirements (if needed). These requirements delimit the feasible ranges of wing and thrust loading in the same manner as for the TAW. All aircraft, irrespective of their configuration, need to achieve the same minimum performance limits set out by regulations. The actual performance of the aircraft during take-off, climb and landing is checked for feasibility with the methods described in Wortmann and Vos.[29] The results of these analyses are not fed back to the determination of the design point and as such have no influence on the design although they demonstrate feasible performance.

C. Drag Estimation

The drag polar of the BWB is estimated using a combination of semi-empirical and numerical methods. Drag is broken down as shown in Eqn. 5 where C_D is the total drag, C_{D_0} is the zero-lift drag, C_{D_w} is the wave drag and C_{D_i} is the induced drag.

$$C_D = C_{D_0} + C_{D_w} + C_{D_i} \tag{5}$$

Zero-lift drag (C_{D_0})is defined following Roskam[26] as the summation of skin-friction drag and pressure drag but excludes wave drag because it is determined separately. The only appropriate methods for this stage of design are the semi-analytical methods which have been developed for conventional aircraft. Both the methods of Torenbeek[18] and Roskam have been previously implemented in the Initiator and shown to have acceptable accuracy. It was however chosen to move forward with that of Roskam since it has increased sensitivity to geometric layout, which is important in the case of a BWB, over the other method or those in literature such as in.[2] Implementation for the outer wing, vertical stabilisers and pylons is the same as for TAW aircraft. It has been chosen to regard the fuselage as a wing lifting surface and using the accompanying equations to determine its C_{D_0}. This is done since the classical fuselage method entails the use of the fineness ratio of a tubular fuselage to fit data.[26] The BWB however does not follow the same trends regarding fuselage area distributions. Base drag is also not present in the same form since the TE of the BWB fuselage ends sharp as for a wing. Furthermore, a TAW fuselage is not responsible for significant lift generation and, as

such, does not present the same pressure drag as a wing would. This parameter is again fitted with the fineness ratio for a TAW in the classical fuselage method which would not be suitable.

Accepting this, the sections of the fuselage between the defined airfoils are treated as trapezoidal wing sections, where the mean thickness, chord, sweep and sectional wetted area are used. The zero lift drag of the fuselage is then determined from Eqn. 6 for the N trapezoidal sections. R_{wf_i} is the interference factor for each section and is assumed to be 1.0 for a flying wing.[26] R_{ls_i} is the correction for a lifting surface determined from a fit for the sectional sweep angle at the maximum airfoil thickness location given in.[26] C_{f_i} is the sectional flat plate skin friction coefficient and is determined using the method given in.[36] Therefore, this method takes the variation of Reynolds number over the rapidly varying chord into account for skin friction. As such, skin friction coefficients should increase along the fuselage span with a decreasing Reynolds number. It must be noted that since it is difficult to estimate the transition point on such a 3D body, which is yet untested with the Initiator, it is chosen to fix the transition point at a Reynolds number of 1 million (as is standard for conventional fuselages). The airfoil thickness location correction factor L' is also detailed in[36] and determined for each section. Lastly, the thickness to chord ratio t/c of the mean geometric chord of each section and the wetted area of the section is used. These sectional drag values are summed and scaled with the reference planform area.

$$C_{D_{0_{\mathrm{f}}}} = \frac{1}{S_{\mathrm{ref}}} \sum_{i=1}^{N} R_{\mathrm{wf}_i} R_{\mathrm{ls}_i} C_{\mathrm{f}_i} \left[1 + L'_i (t/c)_i + 100\,(t/c)_i^4\right] S_{\mathrm{wet}_i} \tag{6}$$

In order to take unaccounted drag effects into account, a miscellaneous drag increase is given in the form of an input percentage of the total C_{D0} according to the method given in.[26] These empirical corrections are based on experience and flight test data of conventional aircraft and are similar to values suggested in.[19] It is expected that BWB aircraft will incur similar penalties as they will also have similar engine installation penalties for example and it is the goal to compare the TAW and BWB using similar methods and penalties when they are applicable.

Wave drag ($C_{D_{\mathrm{w}}}$) is determined following the Delta method laid out by Feagin and Morrison[37] and implemented in the Initiator for conventional aircraft by Vargas.[38] This method has shown better performance in the Initiator than other methods for TAW which are applicable to this level of design and resource availability. Wave drag over the outer wing of the BWB is determined using the routine for a wing surface. For the fuselage it is unknown how well this method can predict the wave drag since it has been formed for straight tapered wings and the fuselage does not conform to this. Furthermore, the fuselage is composed of thick airfoils which incurred unrealistic drag penalties using the wing method. It has also been shown by Sargeant et al. that shockwaves are greatly reduced over the fuselage due to a large pressure relief, making 3D results significantly lower than 2D results.[20] It has been deduced that this effect was not fairly represented by the wing based method and as such also contributed to large overestimations of the fuselage wave drag. Thus it was chosen to treat the fuselage as a conventional fuselage, determining the cross-sectional area distribution including nacelles, pylons and vertical tails, and determining the maximum cross-sectional area. This is then fitted to data for conventional fuselages, resulting in the fuselage wave drag. This is added to the wing wave drag to get the total wave drag.

Induced drag ($C_{D_{\mathrm{i}}}$) has been determined in the Initiator for conventional aircraft using the Athena Vortex Lattice (AVL); a vortex lattice solver which uses the linearised potential flow equations and implemented in the Initiator by.[23] AVL's performance on BWB aircraft in terms of induced drag has also been investigated and used in many studies.[2,14,39,40] The use of AVL also supports the research goals of comparing TAW and BWB using similar methods. The outer wing and fuselage are modelled using the sections and airfoils already defined. Paneling is done similar to conventional aircraft and convergence studies show consistent results at 40 spanwise and 20 chordwise cosine distributed panels. At this stage the trim drag is not yet included because control deflections to achieve trim are too large, leading to erroneous trim drag. As such, the induced drag is expected to increase in future studies.

D. Longitudinal Stability

Preliminary analyses of the aircraft's longitudinal stability and control are made. The location of the aerodynamic centre (AC) for the wing and fuselage combination is determined by AVL. Pitching moment produced also results from AVL. Corrections for the shift in AC due to the nacelles are determined from the conventional TAW methods from Torenbeek.[18] The shift in CG of the aircraft is determined from the

payload loading procedure where the most fore and aft bounds are used for controllability and stability respectively. Neutral static stability is the minimum design goal at this stage due to difficulties in assuring controllability. Stability is assured by a combination of the outer wing sweep and wing location, such that the AC falls on or aft of the most aft CG bound.

IV. Verification and Validation of Methods

The approach to verification of the models is to firstly qualitatively check that the functioning of each routine is logical and follows expected trends from literature. The results are then qualitatively compared to the values that the original authors of the methods attained where this is possible. For validation the results are compared to other BWB design projects that may have used different methods to estimate the same parameters. The BWB test cases used in the verification and validation are the same aircraft used to compare to TAW aircraft, given in Section A and comprise a 150-pax, a 250-pax, and a 400-pax aircraft.

A. Verification

As a first step, the geometry model is verified. This is done qualitatively by checking that the geometry is consistent. It is observed that the cabin planform is unitarily scalable, as intended, and the seating arrangement fits properly within its bounds. Fitting of the center airfoil is robust and results in a tight fit of the cabin box to the bounds of the airfoil with the minimum unpacked space. The oval sections of the pressure shell are correctly formed around the cabin. Different airfoil shapes are shown to result in different radii of the arcs, as intended, and the resulting radii are sufficiently small considering structural stress. These radii can be further adjusted with the h_1 and h_3 settings, which prove to be useful for tweaking the packing efficiency and cargo possibilities. The LE and TE of both the fuselage and outer wing match within 1 mm (XYZ) once convergence has been reached between fuselage and outer wing sizing. Depending on the aircraft at hand, the difference between the oval pressure section and the linear aerodynamic surface can vary from 1 to 5cm. Available area for cargo containers is accurately determined such that the chosen container fits underneath the passenger cabin floor. A cross section through the final fuselage geometry is given in Figure 10 which demonstrates these aspects.

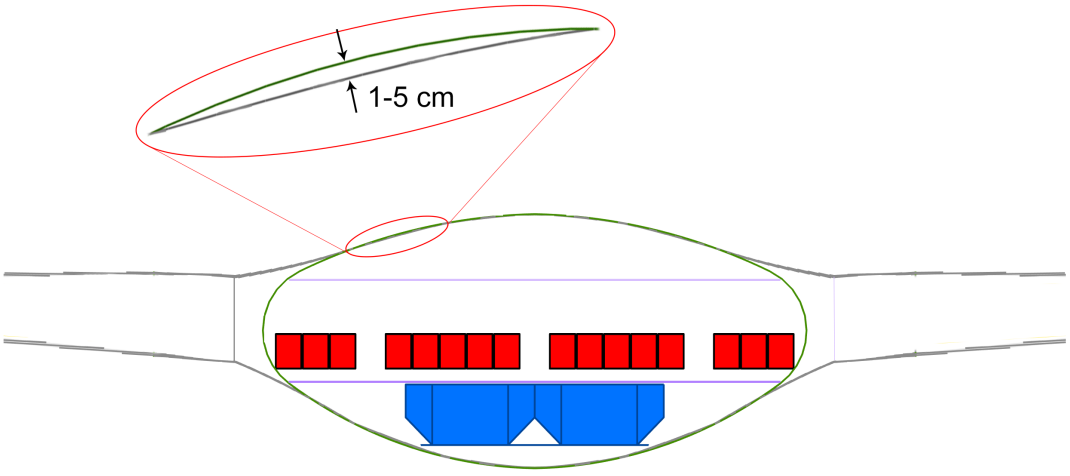

Figure 10 Cross section through the oval fuselage showing the fit of the cabin and cargo with a detail of the difference between the aerodynamic and pressure shell

The Class I mass estimation module functions correctly in that the statistical fits made suitably accommodate the chosen BWB designs. The implemented Class II airframe structural mass estimation from Howe[10] is well verified. Table 1 shows the component masses Howe achieved for the Cranfield BWB, or recommended values when using the method, compared to those of the three Initiator test cases. The results are for aluminum-based aircraft as discussed in Section A. Overall, the total structural mass is well estimated, being similar to that of Howe although still dependent on the actual aircraft geometry. The wing function group is slightly underpredicted where the error seems to be larger for smaller BWBs. This could

be partly due to the idealization issue mentioned before. However it must be clearly noted that Howe's method is based upon a slightly different fuselage structure than the oval fuselage in the Initiator. This is an unavoidable factor and the impact thereof cannot be ascertained but it is likely also a cause for the deviations, especially in the pressure membrane. It is unknown why the door mass seems to be heavily underestimated as the actual area of emergency exits and doors, placed by the cabin sizing routine according to regulations, is used which should result in an accurate door mass. Howe does state that the accuracy of the estimations is within ±5% for $0.4 < y_k < 0.7$ and within ±10% for $0.25 < y_k < 0.9$ where y_k is the ratio of outer wing span to reference span. The Initiator, with the three test cases, results in values of 0.65, 0.68 and 0.69 for y_k which are within the smaller bounds and as such an error of approximately ±5% can be expected. This is reflected in the results and verifies that the mass estimation is functioning as intended.

Table 1 Ratio of airframe component mass to MTOM from Howe and the Initiator

Component	Suggested[10]	Cranfield BWB[10]	BWB150	BWB250	BWB400
Wing Function					
Covers	-	0.093	0.066	0.077	0.088
Ribs	-	0.055	0.041	0.038	0.039
Secondary	-	0.039	0.031	0.031	0.031
Sub total	-	0.186	0.138	0.146	0.158
Fuselage Function					
Nose	0.010	0.009	0.021	0.012	0.009
Press. Membrane	0.010	-	0.044	0.034	0.061
Bulkheads	0.007	-	0.012	0.004	0.004
Pax floor	0.017	-	0.017	0.013	0.015
Cargo floor	-	-	0.003	0.004	0.005
Doors	0.01	-	0.003	0.002	0.002
Windows	0.003	-	0.003	0.003	0.003
Sub total	-	0.055	0.104	0.071	0.099
Total airframe	-	**0.241**	**0.242**	**0.217**	**0.257**

Drag estimations are verified by first comparing the zero-lift drag to the trend in Figure 11. Zero-lift drag is converted to the equivalent skin friction coefficient using the total aircraft wetted area.[19] Results for the BWB fit within the reasonable bounds. Surprisingly, the equivalent skin friction does not tend to monotonically decrease with wetted area as would be expected. This is however also present for the TAW aircraft and does not seem to be an issue inherent to the BWB in the Initiator. It is thus not likely caused by implementation issues with the BWB. This is further substantiated by considering Figure 12 where the skin friction coefficient (not equivalent) found along the span of the BWB is plotted. For the fuselage, due to the sectional implementation of the method (Section C), the skin friction coefficient varies along the span. This is expected since skin friction is a function of Reynolds number.[26] For the outer wing, it is treated as a conventional wing and thus the methods are only applied to the mean geometric chord (MGC). This has been shown to be suitable for a conventional wing[19] and results in similar skin friction coefficients. Induced drag is verified by comparing the results achieved from AVL to that predicted by the classical parabolic drag polar. The results from AVL fit the parabolic curves very closely. Only a slight deviation is present at very low or negative C_L, well below cruise conditions where the induced drag has the largest effect on, for example, the fuel burn. Wave drag is also verified, with parameters used during data interpolation falling between the estimation bounds and the correct determination of the cross-sectional area distribution, approximating the Sears-Haack distribution as expected.

Verification of the longitudinal stability analysis is twofold. First, the determination of the AC of the fuselage-wing combination is verified similarly to the induced drag as it is dependent on the same AVL model. The implementation of the BWB in AVL is compared to the a reference given by Roysdon.[40] Except for the winglets and nacelles, the Intitator model and the reference model are similar. Both use multiple sections to define the planform and kinks are present in both LE and TE, albeit less severe in the reference case. Paneling density seems to be higher in the reference model. Increased panel density was tested in the

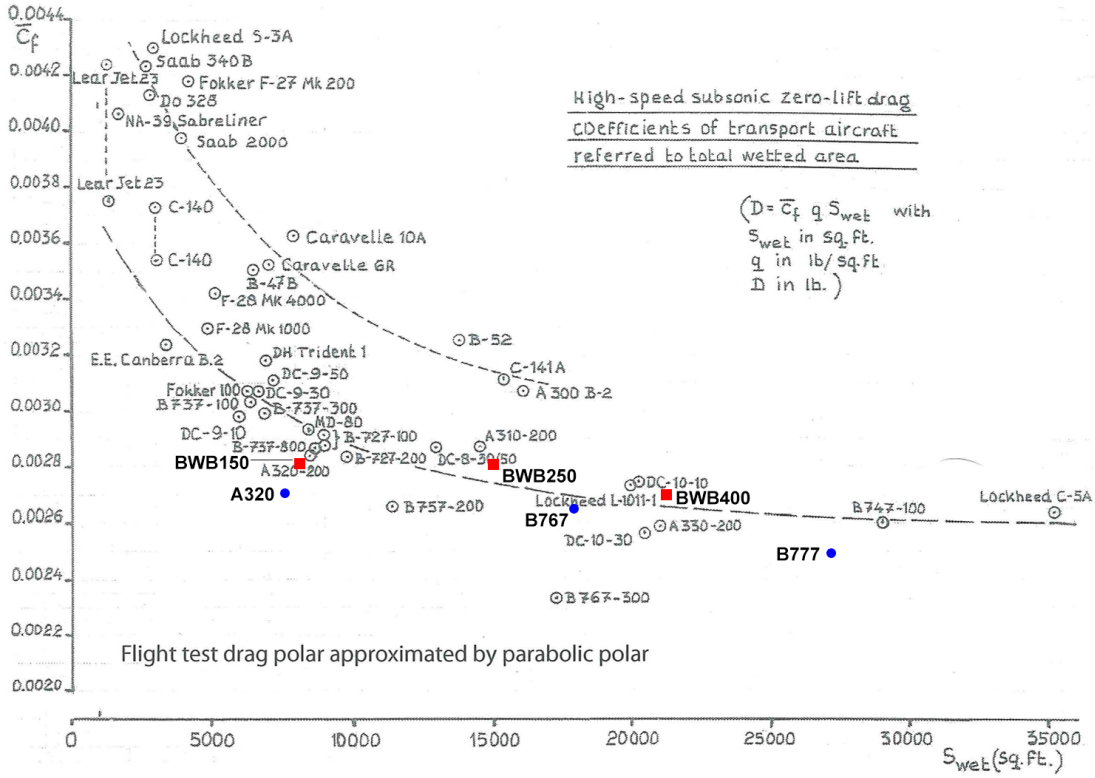

Figure 11 Trend in equivalent skin friction coefficient with wetted area from[19] for conventional aircraft with the results for the BWB from the Initiator

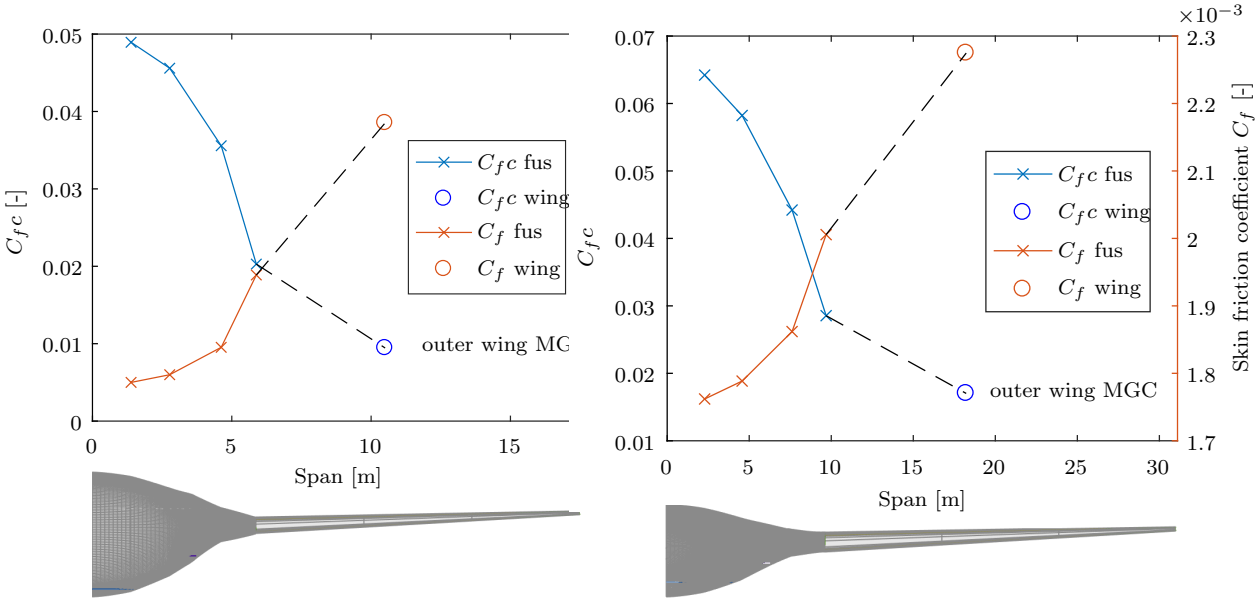

(a) BWB150 (b) BWB400

Figure 12 Skin friction distribution along the span of the fuselage and wing of the BWB400

Initiator but did not result in significant changes in the soloution while requiring longer execution times. Therefore, it is assumed that the aerodynamic model is sufficiently detailed in AVL and that the location of the aerodynamic center is accurately determined to the fidelity at which AVL is intended to perform. Secondly, the corrections for the nacelle are the same as for conventional aircraft and the method was copied and implemented, giving similar results to TAW-aircraft nacelles. This again held true for the range of aircraft tested and, as such, it can be assumed that the model is implemented correctly as it responds as expected.

B. Validation

The geometry parametrization implemented is suitable for modeling a BWB aircraft. A wide range of configurations and aircraft sizes can be modeled, which cover the majority of shapes found in literature. The main aspects of BWB design are present, such as a lifting fuselage with suitable aerodynamic shaping, a pressure cabin in which to carry the payload, adequate layout of this cabin which will carry the passengers and cargo and provision for the remaining of the required aircraft subsystems. Furthermore, the model is adjustable by a combination of automatic and manual design choices which are suitable to conceptual aircraft design. This allows for proper integration with the Initiator and provides all the required data, consistency and flexibility required for subsequent analysis and design. The selected combination of wing loading and thrust-to-weight ratio that results from the performance-constraint analysis is compared to values from other BWB design studies in Figure 13a. The result shows that the Initiator results fall well between the reference values indicating that the method is choosing a suitable design point for the BWB.

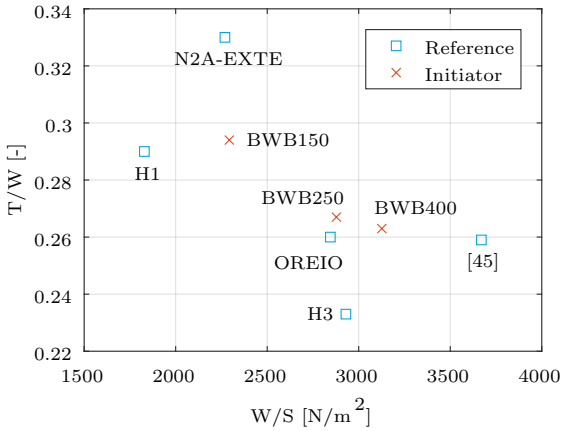

(a) Design wing and thrust loading

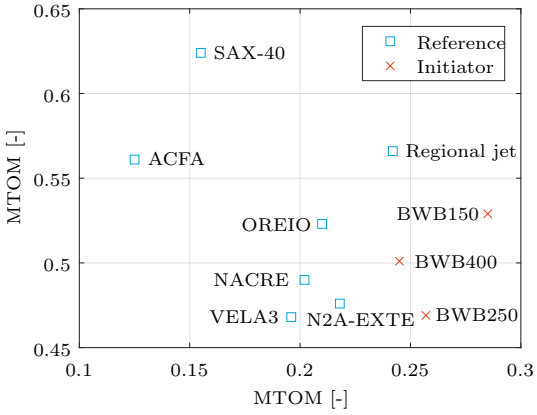

(b) Payload fraction versus OEM fraction

Figure 13 Data for reference BWB aircraft versus the Initiator values

Validation on the mass estimations is be done by comparing the mass results of the Initiator with those found in literature. This is done in Table 2 where three different BWB designs from literature are chosen but available data of complete mass breakdowns is scarce. The results show that the structural mass compares well with reference values. There is a variance of approximately 5% between the three Initiator results, which is in line with the variance present in the reference values showing that the Initiator is within the accuracy bounds that can be expected for a component-mass estimation at the conceptual design stage. Landing gear and fixed equipment are slightly underestimated. However, the operational items are significantly overestimated and it is suspected that part of this mass is taken from the fixed equipment group. The specific division of components to operational and fixed equipment is not given in the reference literature so it could not be cross-checked to the Initiator's division. If the difference between operational items for reference and Initiator aircraft is added to the fixed equipment the values match much better and thus this point is not deemed an issue. This is also supported when the overall OEM fractions are compared, showing quite a spread in reference values and that the Initiator falls within this range. The scatter is also clearly seen in Figure 13b where more reference data is used than in Table 2. This confirms again that the Initiator falls within a feasible OEM range. Interestingly though, it also shows how the Initiator achieves a higher payload efficiency than reference case, on the order of 6%. This could be an underestimation of the overall MTOM

by the Initiator or it shows that the new configuration design logic implemented results in a more compact aircraft, leading to mass reductions. It is believed that a combination of both effects are at play. Overall, it can be said that the mass results are promising and in-line with results from literature and, therefore, deemed fit for this level of design fidelity.

Table 2 Ratio of MTOM of BWB mass components from reference and Initiator aircraft

	OREIO[12]	N2A-EXTE[28]	SAX-40[14]	BWB150	BWB250	BWB400
Structure	0.254	0.241	0.315	0.241	0.225	0.264
Fuselage	0.120	0.144		0.183	0.149	0.185
Wing	0.129	0.078		0.053	0.068	0.071
Vertical tail	0.005	0.019		0.006	0.007	0.008
Landing gear	0.041	0.046	0.044	0.034	0.027	0.029
Engine & nacelle	0.105	0.069	0.111	0.084	0.072	0.070
Fixed equipment	0.133		0.154	0.125	0.110	0.101
Engine systems	0.001			0.009	0.008	0.008
Fuel system	0.019			0.002	0.001	0.001
APU	0.002			0.008	0.008	0.008
Flight cont. & hydraulics	0.025	0.029		0.012	0.009	0.008
Electrical	0.008			0.006	0.003	0.003
Pneumatics & air-con	0.017	0.001		0.002	0.001	0.001
Furnishing and eqpt.	0.012	0.064		0.067	0.064	0.059
Instruments	0.009			0.019	0.015	0.012
Load & handling	0.025					
Empty mass	0.518	0.469		0.484	0.434	0.464
Operational items	0.005	0.007		0.045	0.036	0.037
OEM	0.523	0.476	0.624	0.529	0.469	0.501
Mission fuel	0.267	0.306	0.220	0.185	0.274	0.255
Payload	0.210	0.218	0.155	0.285	0.257	0.245
MTOM [t]	216	214	151	72	170	261

Validation of the drag estimations is done by first comparing the lift-to-drag ratio (L/D) achieved by the Initiator to those achieved by reference BWB studies. Available $(ML/D)_{\max}$ data from literature and results from the Initiator have been laid over those achieved by existing TAW aircraft in Figure 14 taken from Lee et al.[41] The Initiator results for the TAW test cases of Section V are also added. It is immediately clear that the Initiator is underestimating the $(ML/D)_{\max}$ ratio by a significant amount compared to reference BWB which are mostly in the 19-20 range. There is, however, a significant scatter in the reference results (also for TAW) and not all studies fall in the higher$(ML/D)_{\max}$ range. Available breakdowns of the drag components for the reference BWB cases are given in Table 3 along with the Initiator results. It is seen that the Initiator is significantly overestimating the induced and wave drag components. The exact reason cannot be pinpointed. It is assumed that the test case aircraft actually produce a higher induced drag as the SAX-40 study also used AVL to determine the induced drag and the BWB has been correctly modelled in AVL in the current work, in as far as could be verified. The higher wave drag is also accepted as a conservative estimate as they are of the same order of magnitude as reference values and do not represent a very large portion of the total drag. The miscellaneous drag corrections seem to be unnecessary as the zero-lift drag is conservative enough to include these unaccounted drag sources. As such the input miscellaneous drag factors can be lowered in future studies.

The longitudinal stability estimations are difficult to validate since the location of the AC and the pitching moment produced is strongly dependent on the planform geometry of the aircraft. The pitching moment polars of two test-case BWB aircraft are given in Figure 15. The moment response from AVL is linear, as expected, but the values are considered high, especially at higher C_L. Roysdon found moment coefficients of one order of magnitude lower (less negative) while also using AVL.[40] Qin et al., on the other hand, found

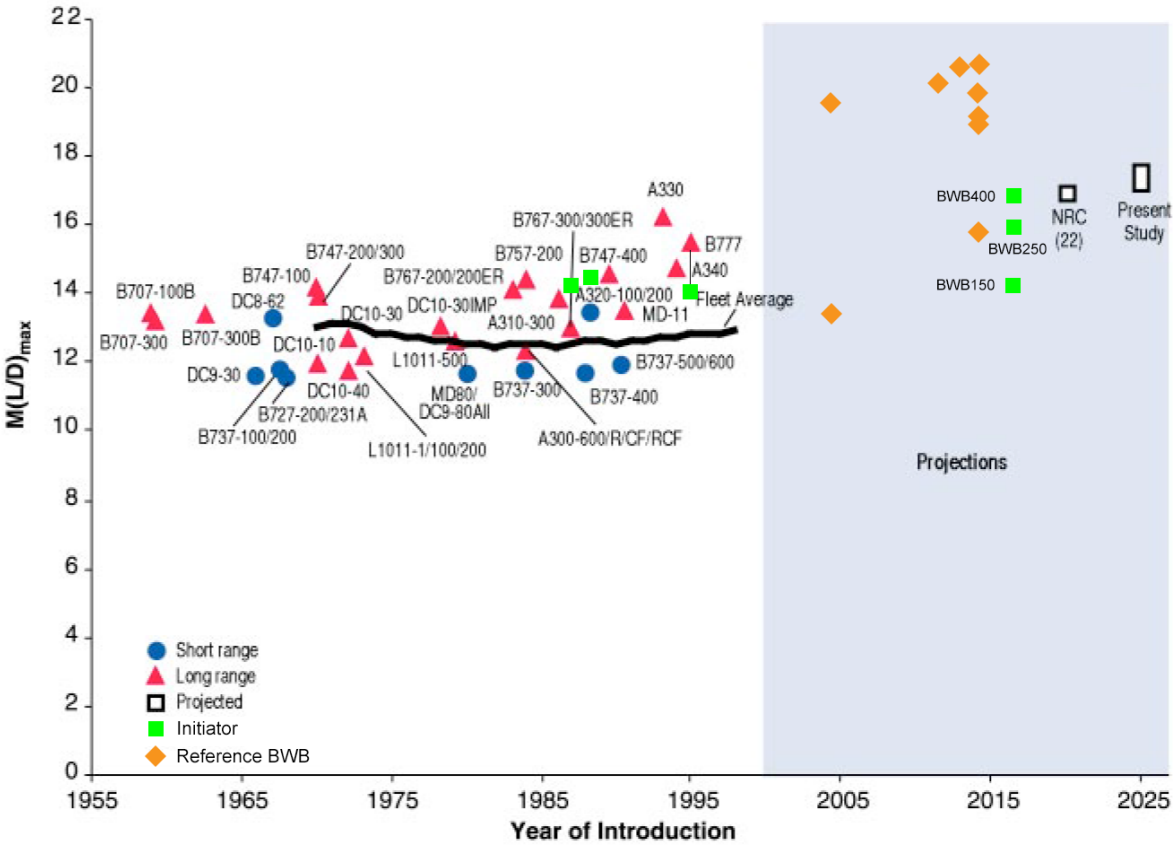

Figure 14 Lift to drag data from Lee et al.[41] combined with reference BWB values from available literature and the results of the Initiator

Table 3 Drag component breakdown comparison between reference and Initiator results
Drag values are in counts [$\times 10^{-4}$]

	SAX-40[14]	OREIO[12]	BWB150	BWB250	BWB400
S_{ref} [m^2]	836	744	308	575	818
$C_{D_{0\ \text{fus}}}$	31	-	44	31	35
$C_{D_{0\ \text{wing}}}$	23	-	18	29	25
$C_{D_{0\ \text{nacelle}}}$	4	-	4	5	6
$C_{D_{0\ \text{v tail}}}$	-	-	2	3	2
C_{D_0}	58	67	67	68	68
$C_{D_{\text{misc}}}$	-	-	11	11	11
$C_{D_{\text{w}}}$	1	1	3	7	8
$C_{D_{\text{i}}}$	24	45	57	54	47
$C_{D\ \text{cruise}}$	82	113	138	141	134
$C_{L\ \text{cruise}}$	0.21	0.27	0.25	0.27	0.26
M	0.80	0.80	0.78	0.80	0.84
$(L/D)_{\text{cruise}}$	25.1	23.5	18.0	19.4	19.1
$(L/D)_{\text{max}}$	25.1	23.5	18.2	19.9	20.0
$M(L/D)_{\text{max}}$	20.2	18.8	14.2	15.9	16.8

values in the range of $C_M = [-0.074 : -0.090]$ in cruise, for initial unoptimized designs using Euler and Navier-Stokes CFD solutions.[42] These values are much closer to the values achieved by the Initiator. The large difference between the references demonstrates the difficulty of accurately predicting pitching moment and the validation thereof. It can be seen that the optimization routine results in a wing sweep such that the moment curves are stable (neutrally for the aft CG), demonstrating that this is functioning functioning properly.

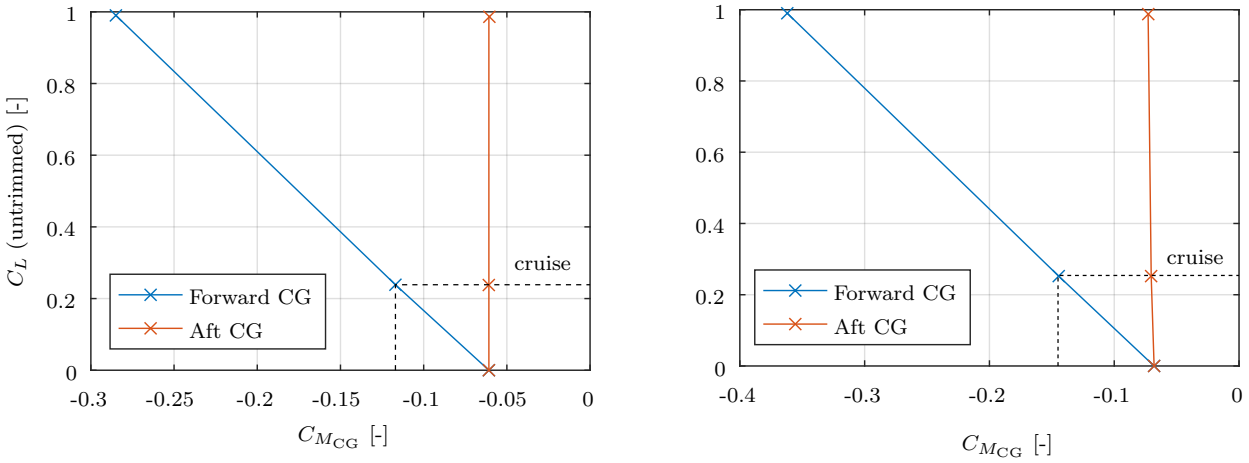

(a) BWB150

(b) BWB400

Figure 15 Trim diagrams for the Initiator BWB aircraft

V. Method Application and Discussion of Results

In this section the results of the analyses between the three different classes of BWB and TAW aircraft is given. Firstly these test cases are presented followed by their requirement analysis and design point results. The mass components of the two concepts are compared where after the drag breakdowns are given and behavior of the drag polars are analyzed for their trends.

A. Test Case Definition: Design Requirements

Considering it is the goal of this work to compare blended wing body aircraft with their conventional tube-and-wing counterparts, the BWB aircraft input TLRs were chosen to be the same as for the TAW aircraft. The choice of test cases is thus based upon the TAW aircraft from each size class in the 150, 250 and 400 pax range, giving a wide analysis of the design space. The selected specifications are taken from the Airbus A320-300, Boeing 767-300ER and the Boeing 777-300, respectively. The input TLRs, design choices, and performance assumptions for each aircraft are summarized in Table 4. Not all aerodynamic performance attributes can be exactly the same between the TAW and the BWB, due to the characteristics of the BWB design and its limitations. This is evident in the $C_{L\ \max}$ values as BWB aircraft are not able to achieve values common for TAW aircraft due to the absence of trailing-edge high-lift devices. Actual $C_{L\ \max}$ values for BWB aircraft are scarce in literature. Kawai has quoted a clean max lift of 0.7 and just over 1.0 with leading edge slats.[28] Van Dommelen and Vos have used a clean value of 1.2 and 1.4 in take-off and landing configuration, respectively.[3] In the present study, a value is chosen between these reference values, which still produces acceptable results with the Initiator. No method is currently implemented which is able to determine the actual $C_{L\ \max}$ of the BWB design at hand thus it is assumed that the assumed value can indeed be achieved. This forms one of the main assumptions of the current work and a weakness in the analyses, which should be taken into account when considering the accuracy of the results. The aspect ratio is chosen considerably lower for the BWB compared to than the TAW aircraft, similar to other BWB design studies.[3,12,25,43] The chosen aspect ratios have been tweaked to achieve good results in terms of wing span for airport gate limits, climb gradients and the resulting sizing of the fuselage and outer wing combination.

The chosen TAW aircraft all use mainly aluminum structures. Therefore, aluminum is also chosen for the BWB aircraft. Lastly, it should be noted that due to the unusual payload-range characteristics of the Boeing 777-300, having a very short harmonic range but very long partial loading range, it was chosen to design the BWB400 with an intermediate range (6700km), representative of other aircraft in this class. For all aircraft a diversion range of 370km and a 30-minute loiter is assumed.

Table 4 Top level requirements, design choices, and performance assumptions for the TAW and BWB test cases

	TAW150	BWB150	TAW250	BWB250	TAW400	BWB400
Pax	156	156	248	248	368	368
Payload [t]	20.5	20.5	43.8	43.8	64	64
Range [km]	3917	3917	7264	7264	3142/12081	6700
Mach	0.78	0.78	0.8	0.8	0.84	0.84
Altitude [m]	11280	11280	10668	10668	10425	10425
Take-off length [m]	2180	2180	2505	2505	3232	3232
Landing length [m]	1840	1430	1660	1660	1838	1838
Airport class [FAR25]	III	III	IV	IV	V	V
BPR	5.70	5.70	5.06	5.06	5.80	5.80
A	9.5	4	8	4.7	8.67	4.8
$C_{L\ \max,\ \text{clean}}$	1.6	1.1	1.4	1.1	1.5	1.1 [t]
$C_{L\ \max,\ \text{TO}}$	2.2	1.3	2.4	1.3	2.1	1.3
$C_{L\ \max,\ \text{L}}$	2.8	1.3	2.6	1.3	2.9	1.3
SFC [lb/hr/lb]	0.6	0.6	0.58	0.58	0.58	0.58

B. Results and Discussion

The requirements listed in Section B have been satisfied for all aircraft tested. The design space for the TAW150 and BWB150 are given in Figures 16a and 16b respectively with the chosen design point in terms of wing loading and thrust-to-weight ratio. The design spaces for all the other aircraft follow the same trends. It can be seen that the design wing loading of the BWB is much lower than that of the TAW as expected. This is due to the much lower $C_{L\ \max}$, which is important for the landing distance requirement. Also, its thrust-to-weight ratio is being constrained by the climb gradient with one engine inoperative and deployed landing gear as given by §FAR25.121a. Climb gradient requirements are harsher for the BWB since it has a lower aspect ratio than the TAW aircraft which negatively affects climb gradient performance.[26] The resulting thrust-to-weight ratio is, however, very close to the TAW aircraft and as such the required engine performance, size, and mass are similar.

The geometry that results from the Initiator for the test case aircraft is shown in Figure 17 for the 150, 250 and 400 pax aircraft, respectively. The TAW and BWB aircraft are plotted to the same scale. It is seen that in all BWB cases the geometry parametrization has been successful in modeling quite different planform shapes and these are by no means the limit of what is possible. One possible weakness with the parametrization is that the location of the joint between the fuselage and outer wing is at the same location for the LE and TE. This limits the layout possibilities slightly as some BWB designs have a more outboard location of the TE kink. Considering the fuselage, the BWB is much shorter, due to its increased cabin width. Diameter or max thickness of the fuselages are quite similar, owing to the same cabin height requirements and the vertical alignment of cabin and cargo bays. The sweep angle of the BWB outer wing is significantly higher than that of the TAW wing due to longitudinal stability limitations. This gives the BWB a wing mass penalty over the TAW. Wing span on the other hand is almost the same although the BWB tends to be span constrained in terms of the airport gate limits.

The overall mass results of the TAW and BWB aircraft are given in Table 5. Results for the BWB and TAW show the masses to be similar although the BWB is marginally lighter than its TAW counterpart. Trends in the mass reductions favor larger aircraft where the best results are achieved in the 250 pax class. The payload mass ratio is also marginally higher for the BWB where the improvements over TAW again

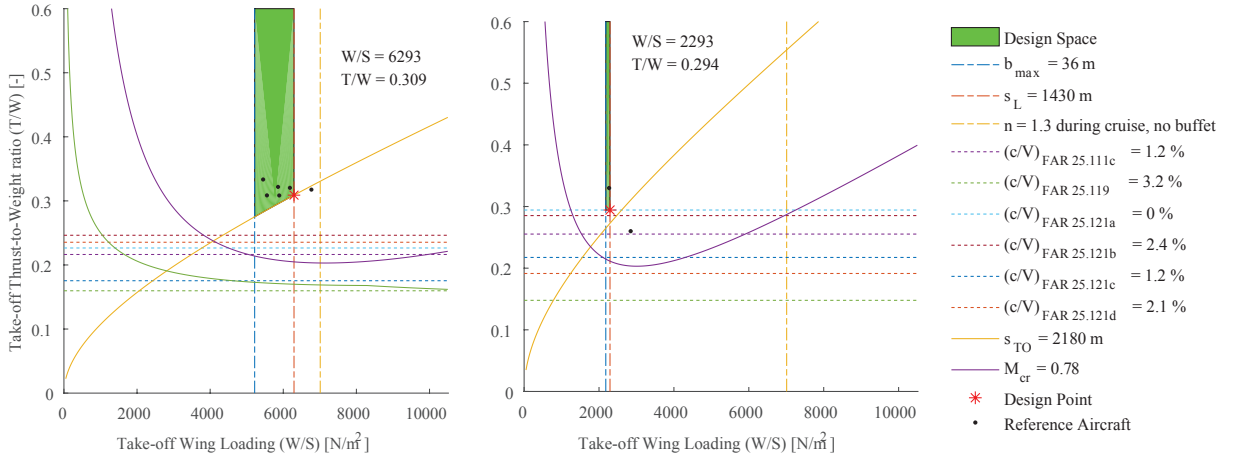

(a) TAW150 (b) BWB150

Figure 16 Constraint diagram showing the feasible design space (in green) and design point in terms of wing loading and thrust-to-weight ratio

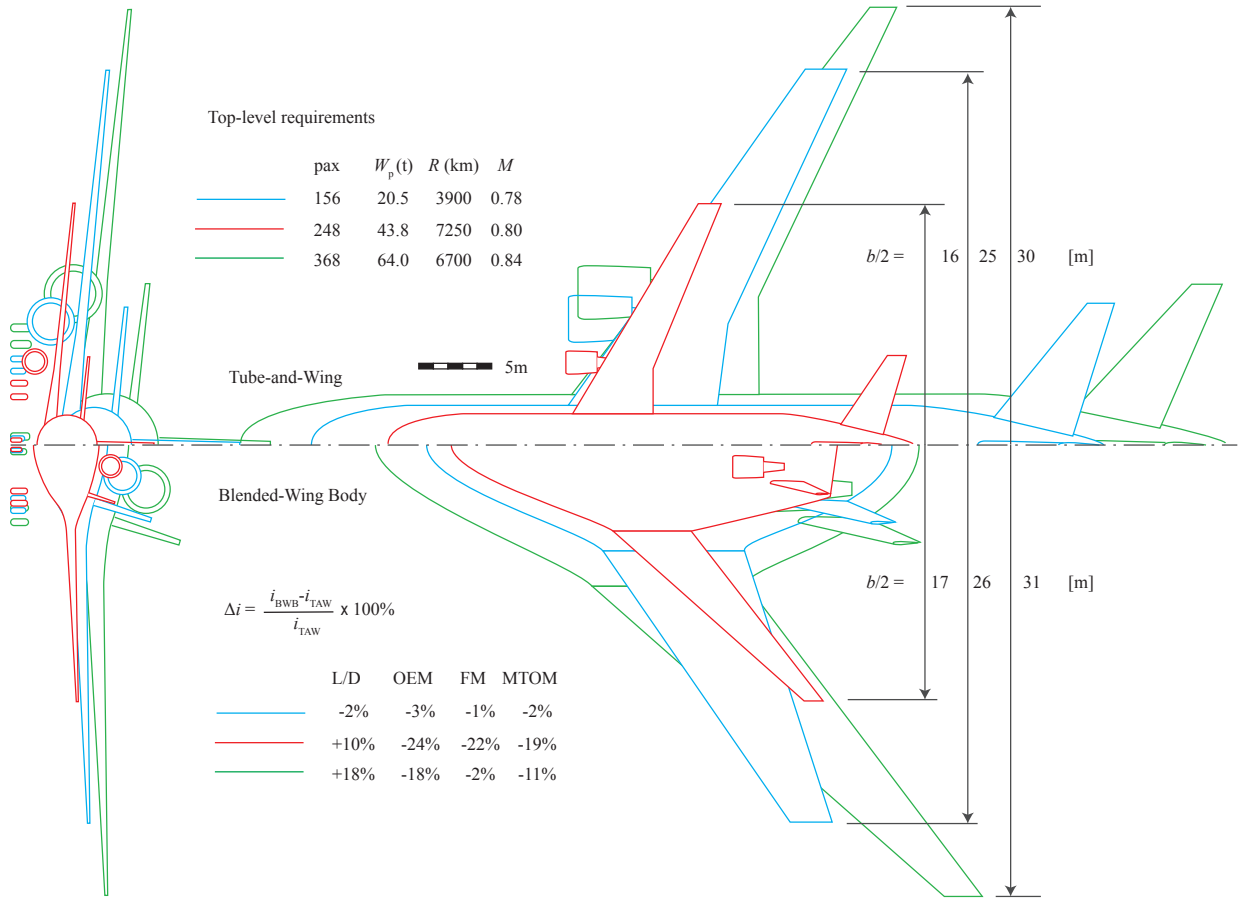

Figure 17 Aircraft geometry and layout for tube-and-wing and blended-wing-body aircraft for three different top-level requirement sets along with the effect on the following performance indicators: aerodynamic efficiency during cruise (L/D), operating empty mass (OEM), fuel mass required to fly the harmonic mission (FM), and maximum take-off mass (MTOM).

increase with aircraft size.

Table 5 Aircraft mass decomposition for the test cases

	TAW150	BWB150	Δ	TAW250	BWB250	Δ	TAW400	BWB400	Δ
PM [t]	21	21	0%	44	44	0%	64	64	0%
OEM [t]	39	38	-3%	106	80	-24%	160	131	-18%
FM_{harmonic} [t]	13	13	-1%	60	47	-22%	68	67	-2%
MTOM [t]	73	72	-2%	209	170	-19%	293	262	-11%
$\frac{\text{OEM}}{\text{MTOM}}$	0.54	0.53	-1%	0.51	0.47	-4%	0.55	0.5	-5%
$\frac{\text{PM}}{\text{MTOM}}$	0.28	0.29	1%	0.21	0.26	5%	0.22	0.24	2%

The drag breakdowns of the TAW and BWB aircraft are given in Table 6. Studying the trend, it is seen that the gains in L/D increase with aircraft size, showing that the BWB is more advantageous at larger aircraft sizes in terms of drag reduction. This result is confirmed by Reist and Zingg[43] who found similar results. It should not be forgotten that it is likely that the Initiator is overestimating the BWB drag (as discussed in Section B) and, in general, underestimating the drag of the TAW (Figures 11 and 14). These factors both stand in favor of the BWB and further supports the evidence that a BWB aircraft is more aerodynamically efficient than a TAW aircraft.

Table 6 Drag decomposition for test case aircraft, all drag values in [cts].

	TAW150	BWB150	TAW250	BWB250	TAW400	BWB400
C_{D_0}	169	67	139	68	150	68
$C_{D_{\text{misc}}}$	14	12	13	12	3	12
$C_{D_{\text{w}}}$	17	3	13	7	62	8
$C_{D_{\text{i}}}$	172	57	170	54	141	47
$C_{D\ \text{cruise}}$	371	138	334	141	356	134
$C_{L\ \text{cruise}}$	0.68	0.25	0.59	0.27	0.57	0.26
L/Dcruise	18.4	18.0	17.7	19.4	16.1	19.1
L/Dmax	18.4	18.2	17.8	19.9	16.3	20.0
$M(L/D)$max	14.4	14.2	14.2	15.9	13.7	16.8
S_{ref} [m^2]	113	308	323	575	431	818

Graphic representations of the drag polars of the test case aircraft are given in Figure 18a. It is clear that the BWB aircraft have very different drag behaviour than TAW. Induced drag rises more quickly with lift due to the lower aspect ratio. This is also confirmed in the L/D polars given in Figure 18b. The BWB also has a steeper peak in L/D than TAW aircraft giving it a smaller high-efficiency $C_{L\ \text{cruise}}$ range. This would have an impact on the cruise profile of the aircraft, requiring more increases in altitude (step climbs) to remain at an efficient C_L. This effect could be reduced by finding a more optimum initial cruise altitude,[1,43] which is left for further research.

VI. Conclusions

A conceptual design methodology for the blended wing body within the semi-automatic design environment of the Initiator has been presented. The methodology allows for the rapid layout, sizing and analysis of a wide range of passenger BWB aircraft. Resulting aircraft can be compared to conventional TAW aircraft that have been sized for the same top level requirements and the performance estimated to the same level of fidelity using similar analysis methods.

It must be clearly noted that while the Initiator is able to consider almost all disciplines, the current implementation for the BWB is not complete and the resulting aircraft are likely to change once these topics are implemented. These include, but are not limited to, longitudinal control, lateral and directional stability and control, high lift estimation, detailed aircraft performance analysis, higher fidelity Class II.5

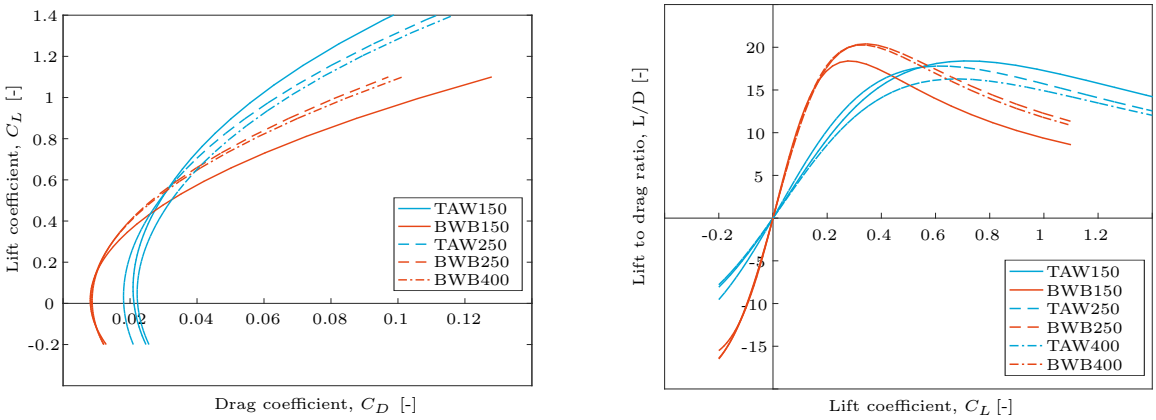

(a) Drag polars

(b) L/D polar

Figure 18 Drag characteristics for the test aircraft

mass analysis and noise production. Mass estimations have been validated to fall within 10% of reference values with 5% difference being common. Drag analyses are overestimating the drag of the BWB. Higher induced drag and penalties to correct for unaccounted drag sources are leading to somewhat lower L/D ratios. Results of the preliminary comparisons between BWB and TAW aircraft tested reveal that the BWB is more aerodynamically efficient than the TAW, especially at larger aircraft sizes. The mass estimations predict the operating empty weight to be lower for a BWB than for a TAW. Together with the higher aerodynamic efficiency, this results in lower fuel burn per passenger kilometer with values as high as 30% for a long-range 250-passenger aircraft. Considering the current level of implementation of the BWB and the coupling between design disciplines that exists, it can be expected that the quantitative results of this study between BWB and TAW will change with further BWB implementation. However the qualitative results and trends should remain valid. The stated improvements of the BWB over the TAW are thus provisional.

References

[1]Okonkwo, P. and Smith, H., "Review of evolving trends in blended wing body aircraft design," *Progress in Aerospace Sciences*, Vol. 82, 2016, pp. 1–23.

[2]Okonkwo, P., *Conceptual Design Methodology for Blended Wing Body Aircraft*, Ph.D. thesis, Cranfield University, 2016.

[3]van Dommelen, J. and Vos, R., "Conceptual design and analysis of blended-wing-body aircraft," *Proceedings of the Institution of Mechanical Engineers, Part G: Journal of Aerospace Engineering*, Vol. 228, doi:10.1177/0954410013518696.

[4]Elmendorp, R., Vos, R., and Rocca, G. L., "A Conceptural Design and Analysis Method for Conventional and Unconventional Airplanes," in "ICAS 2014: Proceedings of the 29th Congress of the International Council of the Aeronautical Sciences," AIAA, St. Petersburg, Russia, 2014.

[5]Nickol, C. L. and McCullers, L. A., "Hybrid Wing Body Configuration System Studies," in "47th AIAA Aerospace Sciences Meeting Including The New Horizons Forum and Aerospace Exposition," AIAA, Orlando, Florida, 2009.

[6]Liebeck, R. H., "Design of the BlendedWing Body Subsonic Transport," *Journal of Aircraft*, Vol. 41, 2004, pp. 10–25.

[7]Nickol, C. L., "Hybrid Wing Body Configuration Scaling Study," in "50th AIAA Aerospace Sciences Meeting including the New Horizons Forum and Aerospace Exposition," AIAA, Nashville, Tennessee, 2012.

[8]Vos, R., Geuskens, F., and Hoogreef, M., "A New Structural Design Concept for Blended Wing Body Cabins," in "53rd AIAA/ASME/ASCE/AHS/ASC Structures, Structural Dynamics and Materials Conference," AIAA, Honolulu, Hawaii, 2012.

[9]Schmidt, K. and Vos, R., "A Semi-Analytical Weight Estimation Method for Oval Fuselages in Conventional and Novel Aircraft," in "52nd Aerospace Sciences Meeting," AIAA, National Harbor, Maryland, 2014.

[10]Howe, D., "Blended wing body airframe mass prediction," *Proceedings of the Institution of Mechanical Engineers, Part G: Journal of Aerospace Engineering*, Vol. 215, 2001, pp. 319–331, doi:10.1243/0954410011533329.

[11]Kanazaki, M., Hanida, R., Nara, T., Shibata, M., Nomura, T., Murayama, M., and Yamamoto, K., "Challenge of design exploration for small blended wing body using unstructured flow solver," *Computers & Fluids*, Vol. 85, 2013, pp. 71–77.

[12]Pitera, D. M., DeHaan, M., Brown, D., Kawai, R. T., Hollowell, S., Camacho, P., Bruns, D., and Rawden, B. K., "Blended Wing Body Concept Development with Open Rotor Engine Integration," Tech. Rep. NASA/CR2011-217303, Boeing and NASA, 2011.

[13]Lyu, Z. and Martins, J. R. R. A., "Aerodynamic Design Optimization Studies of a Blended-Wing-Body Aircraft," *Journal of Aircraft*, Vol. 51, 2014, pp. 1604–1617.

[14]Hileman, J. I., Spakovszky, Z. S., Drela, M., Sargeant, M. A., and Jones, A., "Airframe Design for Silent Fuel-Efficient Aircraft," *Journal of Aircraft*, Vol. 47, 2010, pp. 956–969.

[15]Strüber, H. and Hepperle, M., *Aerodynamic Optimisation of a Flying Wing Transport Aircraft*, Springer Berlin Heidelberg, Berlin, Heidelberg, pp. 69–76, 2006,
doi:10.1007/978-3-540-33287-9_9.

[16]Mason, W., "Analytic models for technology integration in aircraft design," in "Aircraft Design, Systems and Operations Conference," AIAA, Dayton, OH, 1990.

[17]Vargas, J., *Development of a Wave Drag Prediction Tool for the Conceptual Design Phase*, Master's thesis, TU Delft, 2015.

[18]Torenbeek, E., *Synthesis of Subsonic Airplane Design*, Kluwer Academic Publishers, 1982.

[19]Obert, E., *Aerodynamic Design of Transport Aircraft*, IOS Press BV, 2009.

[20]Sargeant, M., Hynes, T., Graham, W., Hileman, J., Drela, M., and Spakovszky, Z., "Stability of Hybrid-WingBody-Type Aircraft with Centerbody Leading-Edge Carving," *Journal of Aircraft*, Vol. 47, 2010, pp. 970–974.

[21]Raymer, D. P., *Aircraft Design: A Conceptual Approach*, American Institute of Aeronautics and Astronautics, 1992.

[22]Larkin, G. and Coates, G., "A design analysis of vertical stabilisers for Blended Wing Body aircraft," *Aerospace Science and Technology*, Vol. 64, 2017, pp. 237–252,
doi:10.1016/j.ast.2017.02.001.

[23]Elmendorp, R., *Synthesis of Novel Aircraft Concepts for Future Air Travel*, Master's thesis, TU Delft, 2014.

[24]Hooker, J. R. and Wick, A., "Design of the Hybrid Wing Body for Fuel Efficient Air Mobility Operations," in "52nd Aerospace Sciences Meeting," AIAA, National Harbor, Maryland, 2014.

[25]Nickol, C. L. and Haller, W. J., "Assessment of the Performance Potential of Advanced Subsonic Transport Concepts for NASAs Environmentally Responsible Aviation Project," in "54th AIAA Aerospace Sciences Meeting," AIAA, San Diego, California, 2016,
doi:10.2514/6.2016-1030.

[26]Roskam, J., *Airplane Design: Part I-VII*, Design, Analysis and Research Corporation, 2008.

[27]Frota, J., Nicholls, K., Whurr, J., Mller, M., Gall, P.-E., Loerke, J., Macgregor, K., Schmollgruber, P., Russell, J., Hepperle, M., Rodriguez, S., Taupin, K., Godard, J.-L., Dron, S., Pltner, K., and Gallant, G., "NACRE - New Aircraft Concepts Research: Final Activity Report 2005 2010," Tech. rep., Airbus SAS, 2011.

[28]Kawai, R. T., "Acoustic Prediction Methodology and Test Validation for an Efficient Low-Noise Hybrid Wing Body Subsonic Transport," Tech. Rep. NF1676L-14465, NASA, 2011.

[29]Wortmann, A., Hoogreef, M., and Vos, R., "Effect of Wing Loading and Fuel Type on Optimal Cruise Altitude for Civil Aircraft," in "15th AIAA Aviation Technology, Integration, and Operations Conference," AIAA, Dallas,TX, 2015.

[30]Torenbeek, E., "The initial calculation of range and mission fuel during conceptual design," Tech. rep., Delft University of Technology, Delft, 1987.

[31]Torenbeek, E., *Advanced Aircraft Design: Conceptual Design, Analysis, and Optimization of Subsonic Civil Airplanes*, John Wiley and Sons, Ltd., 2013.

[32]Mody, P. C., Sato, S., Hall, D. K., de la Rosa Blanco, E., Hileman, J. I., and Wen, E., "Conceptual Design of an N+3 Hybrid Wing Body Subsonic Transport," in "28th AIAA Applied Aerodynamics Conference," AIAA, Chicago, Illinois, 2010.

[33]Velicki, A., Thrash, P., and Jegley, D., "Airframe Development for the Hybrid Wing Body Aircraft," in "47th AIAA Aerospace Sciences Meeting Including The New Horizons Forum and Aerospace Exposition," AIAA, Orlando, Florida, 2009.

[34]Decloedt, D., *Investigation into the Effect of Relaxed Static Stability on a Business Jets Preliminary Design*, Master's thesis, TU Delft, 2016.

[35]Slingerland, A. J., *Development of a Preliminary Sizing Module for Conventional and Unconventional Aircraft*, Master's thesis, TU Delft, 2014.

[36]Boersma, J. Y., *Business Jet Design Using Laminar Flow*, Master's thesis, TU Delft, 2016.

[37]Feagin, R. C. and Morrison, W. D., "Delta method, an empirical drag buildup technique," Tech. Rep. NASA-CR-151971, NASA, 1978.

[38]Vargas, J. A. and Vos, R., "Development of a Wave Drag Prediction Tool for the Conceptual Design Phase," in "54th AIAA Aerospace Sciences Meeting," AIAA, San Diego, California, USA, 2016.

[39]Cusher, A. A. and Gopalarathnam, A., "Drag Reduction Methodology for Adaptive Tailless Aircraft," *Journal of Aircraft*, Vol. 49, 2012, pp. 161–172.

[40]Roysdon, P., "Blended wing body lateral-directional stability investigation using 6DOF simulation," *Proceedings of the Institution of Mechanical Engineers, Part G: Journal of Aerospace Engineering*, Vol. 228, 2013, pp. 7–19,
doi:10.1177/0954410013483633.

[41]Lee, J. J., Lukachko, S. P., Waitz, I. A., and Schafer, A., "Historical and Future Trends in Aircraft Performance, Cost, and Emissions," *Annual Review of Energy and the Environment*, Vol. 26, 2001, pp. 167–200,
doi:10.1146/annurev.energy.26.1.167.

[42]Qin, N., Vavalle, A., Moigne, A. L., Laban, M., Hackett, K., and Weinerfelt, P., "Aerodynamic considerations of blended wing body aircraft," *Progress in Aerospace Sciences*, Vol. 40, 2004, pp. 321–343.

[43]Reist, T. A. and Zingg, D. W., "Aerodynamic Design of Blended Wing-Body and Lifting-Fuselage Aircraft," in "34th AIAA Applied Aerodynamics Conference, AIAA AVIATION Forum," AIAA, Washington, D.C., 2016.